Geosci. Instrum. Method. Data Syst. Discuss., 2, 337–363, 2012
www.geosci-instrum-method-data-syst-discuss.net/2/337/2012/
doi:10.5194/gid-2-337-2012

Discussions
Geoscientific Instrumentation Methods and Data Systems

Solving the orientation problem for an automatic magnetic observatory

A. Khokhlov[1,2], J. L. Le Mouël[2], and M. Mandea[3]

[1]International Institute of Earthquake Prediction Theory and Mathematical Geophysics 79, b2, Warshavskoe shosse, 113556 Moscow, Russia
[2]Institut de Physique du Globe de Paris – UMR7154, 1, Rue Jussieu, 75005 Paris, France
[3]Centre National d'Etudes Spatiales, 2, Place Maurice Quentin, 75001 Paris, France

Received: 12 May 2012 – Accepted: 17 May 2012 – Published: 25 June 2012

Correspondence to: M. Mandea (mioara.mandea@cnes.fr)

Published by Copernicus Publications on behalf of the European Geosciences Union.

Abstract

The problem of the absolute calibration of a vectorial (tri-axial) magnetometer is addressed with the objective that the apparatus, once calibrated, gives afterwards, for a few years, the absolute values of the three components of the geomagnetic field (say the Northern geographical component, Eastern component and vertical component) with an accuracy of the order of 1 nT. The calibration procedure comes down to measure the orientation in space of the three physical axes of the sensor or, in other words, the entries of the transfer matrix from the local geographical axes to these physical axes. Absolute calibration follows indeed an internal calibration which provides accurate values of the three scale factors corresponding to the three axes – and in addition their relative angles. The absolute calibration can be achieved through classical absolute measurements made with an independent equipment. It is shown – after an error analysis which is not trivial – that, while it is not possible to get the axes absolute orientations with a high accuracy, the assigned objective (absolute values of the Northern geographical component, Eastern component and vertical component, with an accuracy of the order of 1 nT) is nevertheless reachable; this is because in the time interval of interest the field to measure are not far from the field prevailing during the calibration process.

1 Introduction

The geomagnetic field is continosly measured in a network of magnetic observatories, which, however, has significant gaps in the remote areas and over the oceans. This uneven distribution is linked to the fact that currently it is not possible to operate fully automated observatories which do not require manual operation of any instrument. Already, some fifty years ago, Alldreage planned an automatic standard magnetic observatory (ASMO) – (Alldregde, 1960; Alldregde and Saldukas, 1964), i.e. a device providing at each time the absolute values of – say – the Northern geographical component,

GID
2, 337–363, 2012

Eastern component and vertical component of the geomagnetic field (without extra independent absolute measurements, at least for a long enough time span). This idea has remained in the geomagnetism community and, over the last years, attempts have been made to automate a DI-theodolite (van Loo and Rasson, 2006), a proton vector magnetometer (Auster et al., 2006) or to build a device which can perform discrete absolute measurements automatically (Auster et al., 2007).

In a former paper (Gravrand et al., 2001), the question was addressed of the internal calibration of a vectorial (or tri-axial) magnetometer, such as the ^{4}He pumped magnetometer built by the laboratoire d'électronique et de technique de l'information (LETI) of the French Commissariat à l'énergie atomique (CEA), or the Oersted space mission fluxgate magnetometer, built by the Institute for automatisation of the Danish Technical University (DTU). The problem of the internal calibration is to determine the six (^{4}He magnetometer) or nine (fluxgate magnetometer) intrinsic parameters: the three scale values (one for each modulation coil physical axis in the ^{4}He case, or each fluxgate sensor axis in the DTU case), the three angles between the three physical axis in both cases, and the three offset values in the case of the fluxgate variometer. The calibration problem can be solved by rotating in space the triaxial magnetometer while making simultaneously absolute intensity measurements with a proton or optical pumping magnetometer (Olsen et al., 2003), and it is essentially linear (Gravrand et al., 2001). The calibration algorithm was developed for ground operation but can be – and has been – extended to in flight calibration. But this internal calibration is not enough if we want to install somewhere a genuine automatic magnetic observatory.

In the following $\boldsymbol{u}_1$, $\boldsymbol{u}_2$, $\boldsymbol{u}_3$ are the unit vectors corresponding to these North-East-Down directions. It was stated in Gravrand et al. (2001) that such an absolute calibration should not be too difficult in a place where standard absolute measurements can be performed. This is the question (of quite practical interest) that we address in the present paper. We show that the above statement is both valid and invalid, depending on the objective. We also show that only the determination of the scale factors provided by the internal calibration process are of interest for the absolute calibration (the accurate determination of all angles between physical axes is not necessary however provided by the internal calibration; see also Appendix).

2 The practical problem

Suppose we want to install an automatic observatory in some new place, say a remote island in the Pacific ocean. What is required is, to refresh Alldredge's statement, to obtain one minute absolute values of the field components X, Y, Z in, say, the North-East-Verical Down frame, fitting Intermagnet standard (see http:/www.intermagnet.org), without needing an observer to visit the place in the few years following the installation.

One first builds a pillar (the permanent pillar) in a location propitious to install the ^{4}He magnetometer, and an auxiliary pillar a few meters apart. The calibration process can start. The observer determines the differences ΔX, ΔY, ΔZ between the absolute values of X, Y, Z at the two pillars. This is classical observatory work, not negligible, but which can be completed in a few days using a DI-flux theodolite and a proton magnetometer; modern devices for determining azimuths are welcome. The magnetometer-variometer, as we call it, can now be installed on the permanent pillar (in fact after a non magnetic house has been built around it; we do not develop here practical aspects). By construction, the unit vectors $\boldsymbol{e}_1$, $\boldsymbol{e}_2$, $\boldsymbol{e}_3$ of the physical axes, or coil axes, of the apparatus are nearly orthogonal, and its installation on the pillar is generally made in such a way that $\boldsymbol{e}_1$ is close to $\boldsymbol{u}_1$, $\boldsymbol{e}_2$ close to $\boldsymbol{u}_2$ and $\boldsymbol{e}_3$ close to $\boldsymbol{u}_3$; although this is by no way a necessary condition. The observer makes at the auxiliary pillar a series of absolute measurements of the magnetic field at time moments t_1, t, ... t_k and corrections ΔX, ΔY, ΔZ are applied to get the corresponding absolute values on the permanent pillar. At the same time moments t_k, the magnetometer-variometer to be calibrated provides the values $\left\{V_k^1, V_k^2, V_k^3\right\}$, $k = 1, 2, \ldots K$ of the components of the magnetic vector $\boldsymbol{V}(t_k)$

GID
2, 337–363, 2012
Orientation problem for an automatic magnetic observatory
A. Khokhlov et al.

along its physical axes $\{\boldsymbol{e}_i\}$ whose orientations with respect to $\{\boldsymbol{u}_1, \boldsymbol{u}_2, \boldsymbol{u}_3\}$, are not exactly known.

The observer, with his equipment, now leaves the place. The magnetometer-variometer in place continues to provide the values $\{V_1(t), V_2(t), V_3(t)\}$ of the (contravariant) components of $\boldsymbol{V}$ along its physical axes. The problem to solve is the following: how, relying on the set of absolute measurements made previously at times t_1, t_2, ... t_k, to compute the geographical components $(X^1(t), X^2(t), X^3(t))$ of $\boldsymbol{V}(t)$ at any following time t (in fact depending on the sampling rate), and estimate the error on those computed values?

This error, as we will see it, is a direct function of the errors on the absolute measurements made at the times t_1, t_2, ... We call it the calibration error. Let us say again that we note $\boldsymbol{B}(t_k)$ the absolute measurements at time t_k and $\boldsymbol{V}(t)$ the measurements provided by the magnetometer-variometer.

3 The principle of the calibration

To compute the $\boldsymbol{e}_i$ vectors in the $\boldsymbol{u}_i$ frame, we go through the $\boldsymbol{B}_k$. Obviously one $\boldsymbol{B}_k$ is not enough; but as a linear operator in R^3 is uniquely defined by its action on three linearly independant vectors, we take three of them, that we note $\boldsymbol{B}_1$, $\boldsymbol{B}_2$, $\boldsymbol{B}_3$, to present the algorithm of the calibration. In practice, several triplets among the K measurements available, if $K > 3$, are used.

Let d_k^j be the geographical components of of $\boldsymbol{B}_k (k = 1, 2, 3)$ (as measured by the observer), and f_k^j the values of the (contravariant) components of $\boldsymbol{B}_k$ along the physical axes $\boldsymbol{e}_1$, $\boldsymbol{e}_2$, $\boldsymbol{e}_3$ provided at the same times by the magnetometer-variometer. We have:

$$\begin{aligned} \boldsymbol{B}_k &= \hat{d}_k^1 \boldsymbol{u}_1 + \hat{d}_k^2 \boldsymbol{u}_2 + \hat{d}_k^3 \boldsymbol{u}_3 \\ \boldsymbol{B}_k &= \hat{f}_k^1 \boldsymbol{e}_1 + \hat{f}_k^2 \boldsymbol{e}_2 + \hat{f}_k^3 \boldsymbol{e}_3 \end{aligned} \quad (1)$$

where the *hat* symbol is to stress the error-free nature of the corresponding quantities. The solution of the calibration is trivial, the $\boldsymbol{e}_i$ being obtained straightforwardly in function of the $\boldsymbol{u}_i$ through the $\boldsymbol{B}_k$:

$$\begin{pmatrix} \boldsymbol{e}_1 \\ \boldsymbol{e}_2 \\ \boldsymbol{e}_3 \end{pmatrix} = \hat{\mathbf{F}}^{-1}\,\hat{\mathbf{D}} \begin{pmatrix} \boldsymbol{u}_1 \\ \boldsymbol{u}_2 \\ \boldsymbol{u}_3 \end{pmatrix} = \hat{\mathbf{C}} \begin{pmatrix} \boldsymbol{u}_1 \\ \boldsymbol{u}_2 \\ \boldsymbol{u}_3 \end{pmatrix} \tag{2}$$

where $\hat{\mathbf{F}}$ and $\hat{\mathbf{D}}$ are the matrices of coefficients (components) $\hat{f}_k^j$ and $\hat{d}_k^j$.

The magnetometer-variometer provides the values and $(V^1(t), V^2(t), V^3(t))$ of the physical componenets of $\boldsymbol{V}$:

$$\boldsymbol{V}(t) = \left(V^1, V^2, V^3\right) \begin{pmatrix} \boldsymbol{e}_1 \\ \boldsymbol{e}_2 \\ \boldsymbol{e}_3 \end{pmatrix} = \left(V^1, V^2, V^3\right) \hat{\mathbf{C}} \begin{pmatrix} \boldsymbol{u}_1 \\ \boldsymbol{u}_2 \\ \boldsymbol{u}_3 \end{pmatrix} = \left(X^1, X^2, X^3\right) \begin{pmatrix} \boldsymbol{u}_1 \\ \boldsymbol{u}_2 \\ \boldsymbol{u}_3 \end{pmatrix}. \tag{3}$$

The problem is solved in the error-free case; we have obtained the geographical componenets (X_1, X_2, X_3) of $\boldsymbol{V}$, at each measurement time. But the problem is in dealing with errors.

4 The errors

4.1 General statements

The absolute measurements of $\boldsymbol{B}_1$, $\boldsymbol{B}_2$, $\boldsymbol{B}_3$ are affected by errors which can be viewed as errors on the geographical components d_k^j of $\boldsymbol{B}_k$ vectors (Eq. 1). They could be discussed at some length; but it is a very well known topic. For the purpose of the present study, we suppose the magnitude of the errors on $\boldsymbol{B}_k$ to be ε in relative value and randomly distributed in direction. In other words:

$$d_k^j\ (\text{measured}) = \hat{d}_k^j\,(\text{true}) + \varepsilon b\, r_k^j.$$

GID
2, 337–363, 2012

Title Page
Abstract | Introduction
Conclusions | References
Tables | Figures
◂| |▸
◂ ▸
Back | Close
Full Screen / Esc
Printer-friendly Version
Interactive Discussion

Here $\varepsilon \ll 1$ and r_k^j are $O(1)$. In matrix form:

$$\mathbf{D} = \hat{\mathbf{D}} + \varepsilon b \mathbf{R}.$$

$\mathbf{R}$ is the matrix of the r_k^j, and b a characteristic value of the $\boldsymbol{B}$ intensity at the station and the epoch of interest.

The values of the components along the physical axes $\{\boldsymbol{e}_i\}$, f_k^j are not either error-free. Nevertheless, in the case of the ^{4}He magnetometer that we have especially in mind, these f_k^j are measured with a very high accuracy, better than 0.1 nT (Gravrand et al., 2001; Léger et al., 2002) after the internal calibration has been performed. To simplify the writing, we consider the values f_k^j as error-free, i.e. $f_k^j = \hat{f}_k^j$ (there is no difficulty nor methodological change when adding errors on f.

It now immediately comes:

$$\mathbf{D}\begin{pmatrix} \boldsymbol{u}_1 \\ \boldsymbol{u}_2 \\ \boldsymbol{u}_3 \end{pmatrix} = \hat{\mathbf{D}}\begin{pmatrix} \boldsymbol{u}_1 \\ \boldsymbol{u}_2 \\ \boldsymbol{u}_3 \end{pmatrix} + \varepsilon b \mathbf{R}\begin{pmatrix} \boldsymbol{u}_1 \\ \boldsymbol{u}_2 \\ \boldsymbol{u}_3 \end{pmatrix} \tag{4}$$

$$\mathbf{D}\begin{pmatrix} \boldsymbol{u}_1 \\ \boldsymbol{u}_2 \\ \boldsymbol{u}_3 \end{pmatrix} = \begin{pmatrix} \boldsymbol{B}_1 \\ \boldsymbol{B}_2 \\ \boldsymbol{B}_3 \end{pmatrix} + \varepsilon b \begin{pmatrix} \boldsymbol{\omega}_1 \\ \boldsymbol{\omega}_2 \\ \boldsymbol{\omega}_3 \end{pmatrix} = \begin{pmatrix} \boldsymbol{B}'_1 \\ \boldsymbol{B}'_2 \\ \boldsymbol{B}'_3 \end{pmatrix} \tag{5}$$

where $\boldsymbol{\omega}_i$, $i = 1, 2, 3$ denote the error along the i-th direction, and $|\boldsymbol{\omega}_i| = O(1)$.

Multiplying Eq. (4) by $\mathbf{F}^{-1}$ (recall that $\mathbf{F}^{-1} = \hat{\mathbf{F}}^{-1}$) and using Eq. (2):

$$\begin{pmatrix} \boldsymbol{e}_1 \\ \boldsymbol{e}_2 \\ \boldsymbol{e}_3 \end{pmatrix} = \mathbf{C}\begin{pmatrix} \boldsymbol{u}_1 \\ \boldsymbol{u}_2 \\ \boldsymbol{u}_3 \end{pmatrix} - \varepsilon b \hat{\mathbf{F}}^{-1}\begin{pmatrix} \boldsymbol{\omega}_1 \\ \boldsymbol{\omega}_2 \\ \boldsymbol{\omega}_3 \end{pmatrix}. \tag{6}$$

In other words, when computing the physical unit vectors $\boldsymbol{e}_i$ using the "measured" transformation matrix $\mathbf{C} = \mathbf{F}^{-1}\mathbf{D}$ (instead of $\hat{\mathbf{C}} = \mathbf{F}^{-1}\hat{\mathbf{D}}$), an error is made which depends

GID
2, 337–363, 2012

Orientation problem for an automatic magnetic observatory

A. Khokhlov et al.

on $\mathbf{F}^{-1}$. The difficulty to be expected is rather obvious. We go from the orthogonal frame $\boldsymbol{u}_i$ to the nearly tri-orthogonal frame $\boldsymbol{e}_i$ through the $\boldsymbol{B}_k$ frame. But the three vectors $\boldsymbol{B}_1$, $\boldsymbol{B}_2$, $\boldsymbol{B}_3$ have directions close to one another (remember that they are measurements made at the station during a time span of say a week (see Sect. 4 for numerical values). The matrix $\mathbf{F}$ whose lines are close to one another is a priori poorly conditionned; its inverse $\mathbf{F}^{-1}$ may have large eigen-values, and a strong amplification of error εb might affect the directions of $\boldsymbol{e}_i$ (i.e. an error on $\boldsymbol{e}_i$ might be amplified and the error on $\boldsymbol{V}(t)$ might be much larger than the error εb on $\boldsymbol{B}_k$ (see Appendix). But, in fact, the practical conditions of the calibration process ($\boldsymbol{B}_k$) and of the following measurements of the current magnetic field $\boldsymbol{V}(t)$ by the magnetometer-variometer discard such error amplification as shown later. We now build a simple algorithm allowing a statistical modeling and providing realistic error estimation, sufficient for the present study.

4.2 A simple algorithm

Let us now consider the vector $\boldsymbol{V}$ at time t. From Eqs. (1), (3) and (5):

$$\boldsymbol{V}(t) = \left(V^1(t), V^2(t), V^3(t)\right) \mathbf{F}^{-1} \begin{pmatrix} \boldsymbol{B}_1 \\ \boldsymbol{B}_2 \\ \boldsymbol{B}_3 \end{pmatrix}$$

$$\boldsymbol{V}'(t) = \left(V^1(t), V^2(t), V^3(t)\right) \mathbf{F}^{-1} \begin{pmatrix} \boldsymbol{B}'_1 \\ \boldsymbol{B}'_2 \\ \boldsymbol{B}'_3 \end{pmatrix}. \tag{7}$$

The $\boldsymbol{B}_k$ are the true values, the $\boldsymbol{B}'_k$ the erroneus absolute measurements of the field at times t_k. $\boldsymbol{V}(t)$ is the true value of $\boldsymbol{V}(t)$ at time t and $\boldsymbol{V}'(t)$ the erroneous measurement of $\boldsymbol{V}(t)$ provided by the magnetometer-variometer due to the error on the determination of the physical axes directions $\boldsymbol{e}_i$. The calibration error on $\boldsymbol{V}(t)$ appears dirrectly as a linear form of the measurement errors on the $\boldsymbol{B}_k$, without explicit reference to the frames $\boldsymbol{u}_i$ and $\boldsymbol{e}_i$:

$$\boldsymbol{V}' - \boldsymbol{V} = \left(V^1, V^2, V^3\right) \mathbf{F}^{-1} \begin{pmatrix} \boldsymbol{B}_1' - \boldsymbol{B}_1 \\ \boldsymbol{B}_2' - \boldsymbol{B}_2 \\ \boldsymbol{B}_3' - \boldsymbol{B}_3 \end{pmatrix} = \alpha_1 \left(\boldsymbol{B}_1' - \boldsymbol{B}_1\right) + \alpha_2 \left(\boldsymbol{B}_2' - \boldsymbol{B}_2\right) + \alpha_3 \left(\boldsymbol{B}_3' - \boldsymbol{B}_3\right). \quad (8)$$

Of course we do not know the true values of $\boldsymbol{B}_1$, $\boldsymbol{B}_2$, $\boldsymbol{B}_3$, but to estimate the error $|\Delta \boldsymbol{V}| = |\boldsymbol{V}' - \boldsymbol{V}|$, it is enough to replace in Eq. (9) the quantities $(\boldsymbol{B}_i' - \boldsymbol{B}_i)$ by their estimates. For that, for a given triplet $\boldsymbol{B}_k$ and a given vector $\boldsymbol{V}$ we resort to a statistical estimate. We consider that the measurement errors $\boldsymbol{B}_i' - \boldsymbol{B}_i$ are randomly and uniformly distributed in a ball of center $\boldsymbol{B}_i'$ and radius εb (Eq. 3). The balls are drawn in dark grey in Fig. 1. Note that the $\boldsymbol{B}_i$ and $\boldsymbol{B}_i'$ can be interchanged, in this error estimation.

5 Numerical results

In this section we estimate the calibration error using the simple algorithm presented above, for different configurations of $\boldsymbol{V}(t)$ and $\boldsymbol{B}_k$, $k = 1, 2, 3$. These vectors are essentially taken or simulated from observatory records. In other words, we estimate the calibration error which would affect the vector data provided by the variometer-magnetometer, in different locations at the Earth's surface.

5.1 Observatory data

We use the hourly means of the three components of the field recorded during the year 1999, as available on the INTERMAGNET CDROM 1999, from four observatories: a high-latitude observatory, Resolute-Bay (RES), an equatorial observatory, Bangui (BNG), and two middle-latitude observatories, one in the Northern and one in the Southern hemispheres, Chambon la Forêt (CLF) and Hermanus (HER). Their coordinates are given in Table 1.

From the theory developed above, it is obvious that the farther apart the $\boldsymbol{B}_k$ are, the better the configuration is for calibration. Then, at a given observatory, the larger the

GID
2, 337–363, 2012

magnetic activity, the larger the possibility for the triplet $\boldsymbol{B}_k$ to be open. To evidence this effect, we select, in 1999, for each observatory O_i, two subsets of 60 days each, $\mathcal{Q}_i$ containing the five quietest days of each month of 1999, and $\mathcal{D}_i$ containing the five most disturbed days. The day selection is made using the Kp indexes (Mayaud, 1980).

5.2 Effect of the (B_1, B_2, B_3) configuration

To study this effect, we take a full day of one-minute values of X, Y, Z from, for example, CLF, specificially the day 6 September 1999, a quiet day belonging to $\mathcal{Q}_{\mathrm{CLF}}$. Figure 2 presents two illustrations of the walk of the vector $\boldsymbol{B}(X, Y, Z)$ during this day (see figure caption).

We form at each minute t the triplet $\boldsymbol{B}_1 = \boldsymbol{B}(t)$, $\boldsymbol{B}_2 = \boldsymbol{B}(t + t_0)$, $\boldsymbol{B}_3 = \boldsymbol{B}(t + 2t_0)$. And, along the lines indicated supra, we associate to each of these triplets a set of vectors $(\boldsymbol{B}'_1, \boldsymbol{B}'_2, \boldsymbol{B}'_3)$, $\boldsymbol{B}'_i$ being in the ball of center $\boldsymbol{B}_i$ and radius εb (Fig. 1).

Note that we have $(1441 - 2t_0)$ triplets $\boldsymbol{B}_k$ (t_0 in minutes). We then compute the calibration error – through formula Eq. (9) – affecting a set of vectors $\boldsymbol{V} = \boldsymbol{W} + \boldsymbol{v}$, $\boldsymbol{W}$ being the mean value of the (recorded) field for day 6 September 1999, and $\boldsymbol{v}$ a vector uniformly distributed in a ball of center $\boldsymbol{W}$ and radius δb (the big light grey ball of Fig. 1); note that the set of vectors $\boldsymbol{V}$ is partly simulated. We compute, for a given calibration triplet $\boldsymbol{B}_k$, the mean value of $|\Delta \boldsymbol{V}| = |\boldsymbol{V}' - \boldsymbol{V}|$ (Eq. 9) and its maximum value taken on the set of $(\boldsymbol{B}'_1, \boldsymbol{B}'_2, \boldsymbol{B}'_3)$ and the set of $\boldsymbol{V}$. Those quantities $|\Delta \boldsymbol{V}|_{\mathrm{av}}$ and $|\Delta \boldsymbol{V}|_{\mathrm{max}}$ are in this way computed for each of the $\boldsymbol{B}_k$ triplets $\boldsymbol{B}_1 = \boldsymbol{B}(t)$, $\boldsymbol{B}_2 = \boldsymbol{B}(t + t_0)$, $\boldsymbol{B}_3 = \boldsymbol{B}(t + 2t_0)$, for the $(1441 - 2t_0)$ values of t, as defined above. We are left with the populations $|\Delta \boldsymbol{B}|_{\mathrm{av}}(t)$ and $|\Delta \boldsymbol{B}|_{\mathrm{max}}(t)$. We order them using a parameter η which grossly characteristizes the quality of the configuration $\boldsymbol{B}_k$, i.e. the aperture of this triplet. We choose:

$$\eta = \left| \left\langle \frac{\boldsymbol{B}_1}{|\boldsymbol{B}_1|}, \frac{\boldsymbol{B}_2 - \boldsymbol{B}_1}{|\boldsymbol{B}_2 - \boldsymbol{B}_1|}, \frac{\boldsymbol{B}_3 - \boldsymbol{B}_1}{|\boldsymbol{B}_3 - \boldsymbol{B}_1|} \right\rangle \right| = \frac{\left| \left\langle \boldsymbol{B}_1, \boldsymbol{B}_2, \boldsymbol{B}_3 \right\rangle \right|}{|\boldsymbol{B}_1| \cdot |\boldsymbol{B}_2 - \boldsymbol{B}_1| \cdot |\boldsymbol{B}_3 - \boldsymbol{B}_1|}. \tag{9}$$

Discussion Paper | Discussion Paper | Discussion Paper | Discussion Paper |

GID

2, 337–363, 2012

Orientation problem for an automatic magnetic observatory

A. Khokhlov et al.

$< >$ is for the mixt product. Figure 3 represents the distribution of $|\Delta \boldsymbol{B}|_{\text{av}}(t)$ and $|\Delta \boldsymbol{B}|_{\text{max}}(t)$ versus η. The parameter η is not discriminant enough to rank univoqually the $|\Delta \boldsymbol{B}|(t)$ distribution; many points of the plot have the same abscissa. Nevertheless, it appears clearly that the calibration errors $|\Delta \boldsymbol{B}|_{\text{av}}(t)$ and $|\Delta \boldsymbol{B}|_{\text{max}}(t)$ decrease when η increases.

5.3 Histograms of the calibration error

We now present some reciprocal numerical experiments, closer to the real situation to be met, using again minute data of day 6 September 1999. This time we choose a single absolute measurement triplet $\boldsymbol{B}_k$, $k = 1, 2, 3$, picked up in the observatory records, specificially at $t = 0300, 0600, 1500$ on 6 September 1999, and retain as current vectors $\boldsymbol{V}(t)$ all the one-minute values recorded at CLF over the 1999 year (instead of the simulated vectors in the ball of center $\boldsymbol{W}$). Again a set of triplets $(\boldsymbol{B}'_1, \boldsymbol{B}'_2, \boldsymbol{B}'_3)$ is associated with $(\boldsymbol{B}_1, \boldsymbol{B}_2, \boldsymbol{B}_3)$, uniformly distributed in a ball of radius εb centered respectively at $(\boldsymbol{B}_1, \boldsymbol{B}_2, \boldsymbol{B}_3)$. For each vector $\boldsymbol{V}(t)$ (1441 of them) we compute the average and maximum values of $|\Delta \boldsymbol{V}|$ over the set of $(\boldsymbol{B}'_1, \boldsymbol{B}'_2, \boldsymbol{B}'_3)$. The histograms of the set of $|\Delta \boldsymbol{V}|_{\text{av}}(t)$ and $|\Delta \boldsymbol{V}|_{\text{max}}(t)$ are shown in Figs. 4 and 5 for $\varepsilon b = 0.75, 1, 2$ nT. It appears that $|\Delta \boldsymbol{V}|_{\text{av}}(t)$ (the most realistic estimate), for $\varepsilon b = 1$ nT, is most of the time smaller than 2 nT (Fig. 5).

In Fig. 6 $|\Delta \boldsymbol{V}|_{\text{max}}(t)$ values are simply ranked versus time t. An examination of this figure in regard of the magnetic situation shows that, as expected, the largest values of $|\Delta \boldsymbol{V}|_{\text{max}}(t)$ are associated with magnetic storms: $\boldsymbol{V}(t)$, during these events, leaves the ball of centre $\boldsymbol{W}$ and radius δb (Fig. 1; $\delta b = 50$ nT). Note in passing that it is not important, in general, to know with a high accuracy the absolute value of $\boldsymbol{V}(t)$ at each minute of a magnetic storm.

5.4 Time tables

We now give, for each of our four observatories, a different presentation of the calibration error, more practical, which gives the time-spans during which this error is

GID
2, 337–363, 2012

smaller than a given threshold of αnT. We choose again values of year 1999, consider the triplets $\boldsymbol{B}_1 = \boldsymbol{B}(t)$, $\boldsymbol{B}_2 = \boldsymbol{B}(t+t_0)$, $\boldsymbol{B}_3 = \boldsymbol{B}(t+2t_0)$, and compute the corresponding calibration errors $|\Delta \boldsymbol{B}|_{av}(t)$ as explained in the last but one paragraph. Figures 7 to 11 present the results for the four observatories; values of the parameters are given in the captions. All graphs – that we call time tables – are to be read in the following way: the upper sub-panel (in blue) is for the 60 most disturbed days of the year, the lower one (in red) for the 60 quietest days. In each of the sub-panels the days are ranked as follows: the five quietest days of January, according to their calendar date are at the bottom of the lower sub-panel, the five quiestet days of December at its top.

In Figs. 7 to 10 the considered value is $\alpha = 2$ nT. In Fig. 11, relative to Bangui, a time table for $\alpha = 4$ nT is also presented. Everywhere $t_0 = 7.5$ h for the upper panels, $t_0 = 6.0$ h for the lower panels. Of course, $t < 0900$ for $t_0 = 7.5$ h $(24 - 2 \times 7.5)$, and $t < 1200$ for $t_0 = 6.0$ h. In all the computations $\varepsilon b = 1$ nT and $\delta b = 50$ nT We plot a characteristic function which is equal to zero at time t (white) if the triplet ($\boldsymbol{B}_1 = \boldsymbol{B}(t)$, $\boldsymbol{B}_2 = \boldsymbol{B}(t+t_0)$, $\boldsymbol{B}_3 = \boldsymbol{B}(t+2t_0)$) leads to a $|\Delta B|$ error >2 nT; otherwise, a colored tiret, red or blue, is drawn. Continous red or blue time intervals are such that, for any first measurement with t in this interval, leads to a calibration error smalles than 2 nT on $\boldsymbol{V}(t)$.

Looking at graphs of Figs. 7 to 10, we remark, as expected, that it is easier to get time intervals with $\Delta < 2$ nT for the disturbed days than for the quiet days, and for a high latitude observatory (RES) than for an equatorial one (BNG). Figure 11 is an exemple of the effect of changing t_0.

6 Discussion and conclusion

Stability in absolute values, and particularly long term stability – say up to a few years – used to be the most difficult requirement to fulfill in magnetic observatories. Let us adopt the standards of the INTERMAGNET program, which are up to now essentially intended to classical observatories with regular (generaly weekly) man-made absolute

GID
2, 337–363, 2012

measurements. The values provided by the magnetometer-variometer should be exact in absolute value within a few nT (it is said 5 nT in 99 % of cases). From the results of Sect. 4, it appears that, after the calibration performed as in Sects. 2 and 3, the magnetometer-variometer – as already said, we have especially in mind the LETI (CEA) apparatus – can function as an automatic observatory fitting INTERMAGNET standards for a time-span of one to a few years, depending on the amplitude of the secular variation. A special study is necessary in the case of the highest latitude observatories. The necessity of a visiting the station every other year or so to renew the calibration is not so hard a constraint; in any case, such visits should be necessary for other purposes and checkings. We conclude with three remarks, of different nature, which could not be developed in this paper.

First, we have to stress that we only discussed the effect of the inaccuracy of the absolute measurements of $\boldsymbol{B}_k$ on the values $\boldsymbol{V}$ given subsequently by the magnetometer supposed to remain identical to itself, in particular geometrically invariant. The ^{4}He magnetometer is built in such a way as to ensure this stability. We do not discuss either the important question of the stability of the pillar.

Second, we stress again that we only made an excursion in the (calibration) error space, using the simple algorithm described in Sect. 4. A full exploration of this space would be a heavier task; in the Appendix we give a glimpse of it.

The third remark, that we already touched upon in Sect. 5 is, although relevant to he problem at hand, more general. Long term stability generally is required for the study of long time scale phenomena (secular variation of the main field, solar cycle related variations, seasonal variations). For this kind of studies what is relevant is not the absolute accuracy of one-minute values, but of some means (annual, monthly, daily, hourly); and, briefly speaking, averaging reduces the error.

A full understanding of the Earth's magnetic field will come from improvements in measuring it and separating its different componenets with a better spatial and temporal resolution. The upcoming ESA Swarm mission will provide the best-ever survey of the

GID
2, 337–363, 2012

geomagnetic field and its temporal evolution. This constellation will benefit from a new generation of instruments, as each satellite will carry two ^{4}He magnetometers.

We first give some upper bound of the error amplification in the case there is no restriction on the current vector $\boldsymbol{V}(t)$. We start from Eq. (1), $\boldsymbol{B}_k = \mathbf{F}\,(\boldsymbol{e}_1, \boldsymbol{e}_2, \boldsymbol{e}_3)^T$ (T for transposed) and define here the amplification as the ratio of the directionnal error on the physical axes $\boldsymbol{e}_i$ to the directionnal error on the $\boldsymbol{B}_k$ vectors of the calibration triplet. Consider the two triangles whose summits are the extremities of $(\boldsymbol{e}_1, \boldsymbol{e}_2, \boldsymbol{e}_3)$ and $(\boldsymbol{B}_1, \boldsymbol{B}_2, \boldsymbol{B}_3)$, respectively (Fig. 1). From Eq. (1), we can express the $\boldsymbol{e}_i$ versus the $\boldsymbol{B}_k$ through $\mathbf{F}^{-1}$ matrix, and vectors $(\boldsymbol{e}_l - \boldsymbol{e}_m)$ in terms of vectors $(\boldsymbol{B}_i - \boldsymbol{B}_j)$ (in fact two of them, since the sum of the three differences is zero). The lengths of vectors $(\boldsymbol{e}_l - \boldsymbol{e}_m)$ are $\approx \sqrt{2}$, and the lengths of the $\boldsymbol{B}_i - \boldsymbol{B}_j$ of the order of δb, as given in the main text. Therefore $\mathbf{F}^{-1}$ transforms $(\boldsymbol{B}_1, \boldsymbol{B}_2, \boldsymbol{B}_3)$ triangle sides into $(\boldsymbol{e}_1, \boldsymbol{e}_2, \boldsymbol{e}_3)$ triangle sides (Fig. 1 of the main text) through factors of the order of $(\delta b)^{-1}$. If the direction of some of the measurement errors $\varepsilon b \boldsymbol{\omega}_i$ (Eq. 5) happens to be close to that of one of the sides $(\boldsymbol{B}_i - \boldsymbol{B}_j)$, the corresponding error on the $|\boldsymbol{e}_l - \boldsymbol{e}_m|$ will be multiplied by a factor $(\delta b)^{-1}$. Directional errors on the $\boldsymbol{e}_i$ result which are of the order of $(\delta b)^{-1}\,\varepsilon b = \varepsilon/\delta \approx 50^{-1}$; the amplification of the directionnal error ε on the $\boldsymbol{B}_k$ is then $(\delta)^{-1} \approx 10^3$, with the value of the (δb) adopted in the main text. This estimate of the maximum amplification can be obtained through a more rigorous analysis using operator theory. We do not present it.

In the numerical experiments of the main text, we did not observe strong amplifications of the error on the current vector $\boldsymbol{V}(t)$ compared to the error εb on the calibation vectors $\boldsymbol{B}_k$ (see e.g. histograms of Figs. 4 and 5). The reason is as follows: all vectors $\boldsymbol{V}(t)$ are supposed to belong to a rather small neighborhood of the vector $\boldsymbol{B}_k$ which can also be characterized by the quantity εb. In other words, $(\boldsymbol{V}^1, \boldsymbol{V}^2, \boldsymbol{V}^3)$ is close, within b, of (f_1^1, f_1^2, f_1^3), (f_2^1, f_2^2, f_2^3), (f_3^1, f_3^2, f_3^3), like these three triplets are close to one another. It results that the coefficients α_1, α_2, α_3 of Eq. (9) of our practical algorithm are close enough to 1. No large amplification of error arises, even if the $\boldsymbol{e}_i$ are not accurately determines. These considerations shed light on the statement of the introduction that

Discussion Paper | Discussion Paper | Discussion Paper | Discussion Paper |
GID
2, 337–363, 2012
Orientation problem for an automatic magnetic observatory
A. Khokhlov et al.

absolute calibration should not be too difficult: it is true for the objectives of an automatic magnetic observatory, not in general.

Acknowledgements. The results presented in this paper rely on data collected at geomagnetic observatories. We thank the national institutes that support them and INTERMAGNET for promoting high standards of magnetic observatory practice. We also thank Mike Rose who agreed to serve as Associate Editor.

References

Alldregde, L. R.: A proposed automatic standard magnetic observatory, J. Geophys. Res., 65, 3777–3786, 1960.

Alldregde, L. R. and Saldukas, I.: An automatic standard magnetic observatory, J. Geophys. Res., 69, 1963–1970, 1964.

Auster, H. U., Mandea, M., Hemshorn, A., Pulz, E., and Korte, M.: Automation of absolute measurement of the geomagnetic field, Earth Planet. Space, 59, 1007–1014, 2007.

Auster, V., Hillenmaier, O., Kroth, R., and Weidemann, M.: Proton Magnetometer Development, XIIth IAGA Workshop on Geomagnetic Observatory Instruments, Data Acquisition and Processing, Abstract volume, 56, Instytut Geofizyki Polskiej Akademii, Poland, 2006.

Gravrand, O., Khokhlov, A., Le Mouël, J.-L., and Léger, J.-M.: On the Calibration of a Vectorial ^{4}He Pumped Magnetometer, Earth Planet. Space, 53, 949–958, 1960.

Léger, J.-M., Kervnevez, N., and Morbieu, B.: Developement of a laser pumped helium magnetometer, Undersea Defence Technology conference proceedings, 831–835, UDT 92, London, UK, 1992.

Mayaud, P. N.: Derivation, meaning, and use of geomagnetic indices, Geophysical Monograph Series of American Geophysical Union, edited by: Spilhaus Jr., A. F., Geophysical Monograph 22, Am. Geophys. Union, Washington, D.C., 1980.

Olsen, N., Toffner-Clausen, L., Sabaka, T., Brauer, P., Merayo, J. M., Jorgensen, J. L., Léger, J., Nielsen, O. V., Primdahl, F., and Risbo, T.: Calibration of the Ørsted vector magnetometer, Earth Planet. Space, 55, 11–18, 2003.

Van Loo, S. A. and Rasson, J. L.: Presentation of the prototype of an automatic DI-Flux, XIIth IAGA Workshop on Geomagnetic Observatory Instruments, Data Acquisition and Processing, Abstract volume, 21, Instytut Geofizyki Polskiej Akademii, Poland, 2006.

Table 1. The magnetic observatories used in this study.

N		IAGA code	Latitude	Longitude
1	Resolute Bay	RES	74.69	265.11
2	Chambon la Forêt	CLF	48.02	2.27
3	Bangui	BNG	4.33	18.57
4	Hermanus	HER	−34.43	19.23

GID
2, 337–363, 2012

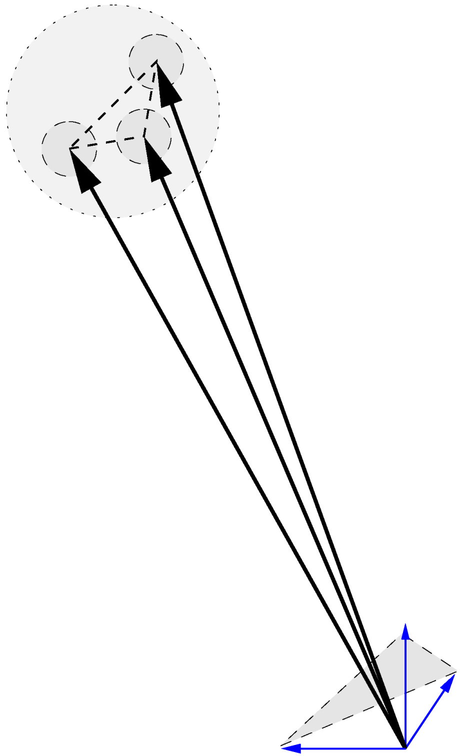

Fig. 1. Calibration triplet $\boldsymbol{B}_1$, $\boldsymbol{B}_2$, $\boldsymbol{B}_3$ and the geographical North-East-Down frame $\{\boldsymbol{u}_i\}$. The unit vectors $\boldsymbol{e}_1$, $\boldsymbol{e}_2$, $\boldsymbol{e}_3$ (defining the physical axes) are nearly orthogonal, and each $\boldsymbol{e}_i$ is close to corresponding $\boldsymbol{u}_i$. Large gray ball represents the variation of vector $\boldsymbol{V}$ (the one to be measured after calibration); small balls radii represent the measurement error εb; value δb is the upper bound for all $|\boldsymbol{B}_i - \boldsymbol{B}_k|$, i, $k = 1, 2, 3$.

GID
2, 337–363, 2012

Orientation problem for an automatic magnetic observatory

A. Khokhlov et al.

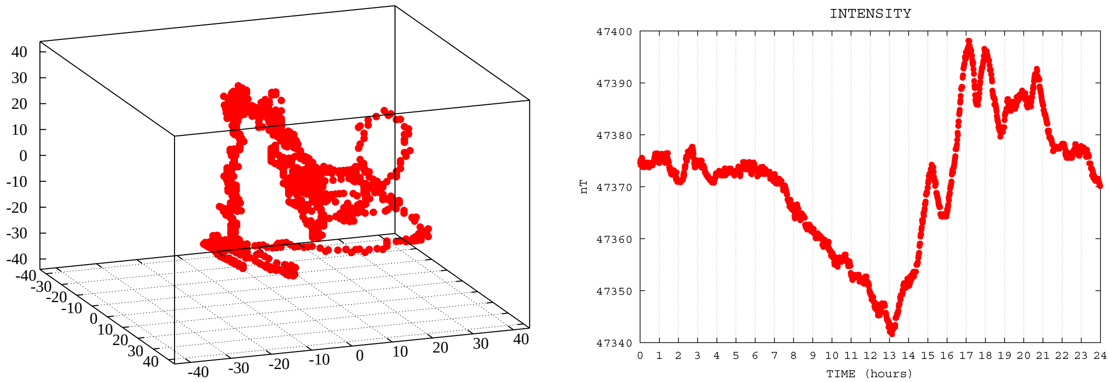

Fig. 2. Magnetic vector evolution (in nT) for the record CLF (6 September 1999): in 3-D frame centered to its mean (left panel), intensity only (right panel).

GID
2, 337–363, 2012

Orientation problem for an automatic magnetic observatory

A. Khokhlov et al.

Title Page
Abstract | Introduction
Conclusions | References
Tables | Figures
◀| |▶
◀ ▶
Back | Close
Full Screen / Esc
Printer-friendly Version
Interactive Discussion

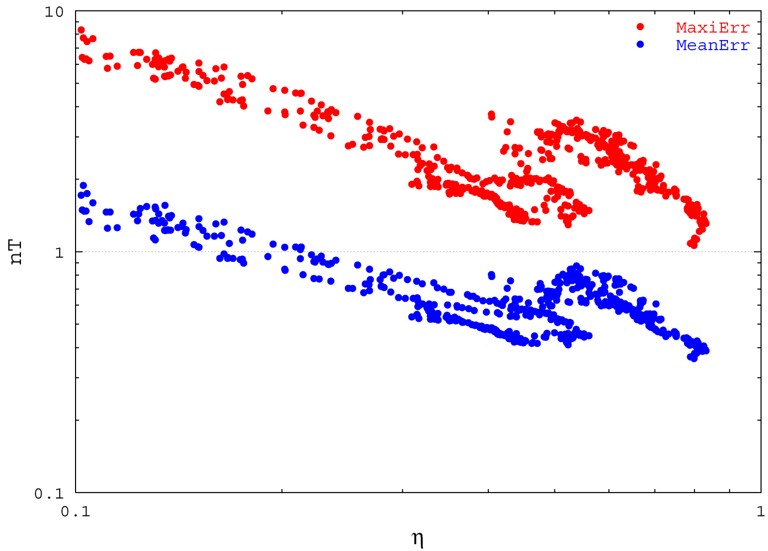

Fig. 3. Data CLF [06.09.1999]. Calibration errors (maximum and average) in nT for $|\boldsymbol{v}| = 50$ nT, $\varepsilon b = 0.75$ nT, delay $t_0 = 6$ h.

GID
2, 337–363, 2012

Orientation problem for an automatic magnetic observatory

A. Khokhlov et al.

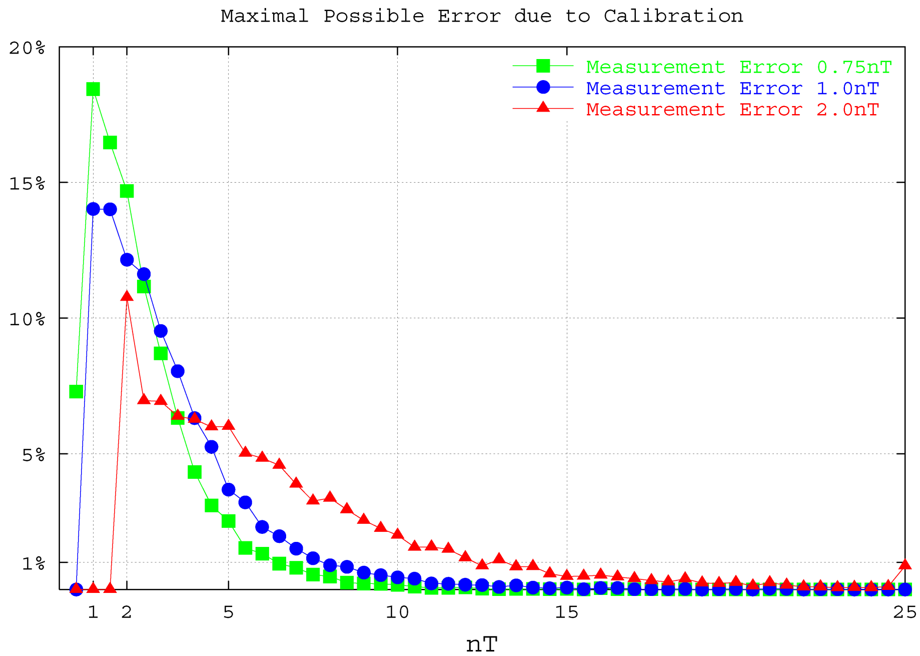

Fig. 4. Normalized histograms of the observed errors for CLF observatory during 1999: the maximal possible error for $\varepsilon b = 0.75, 1, 2\,\text{nT}$.

GID
2, 337–363, 2012

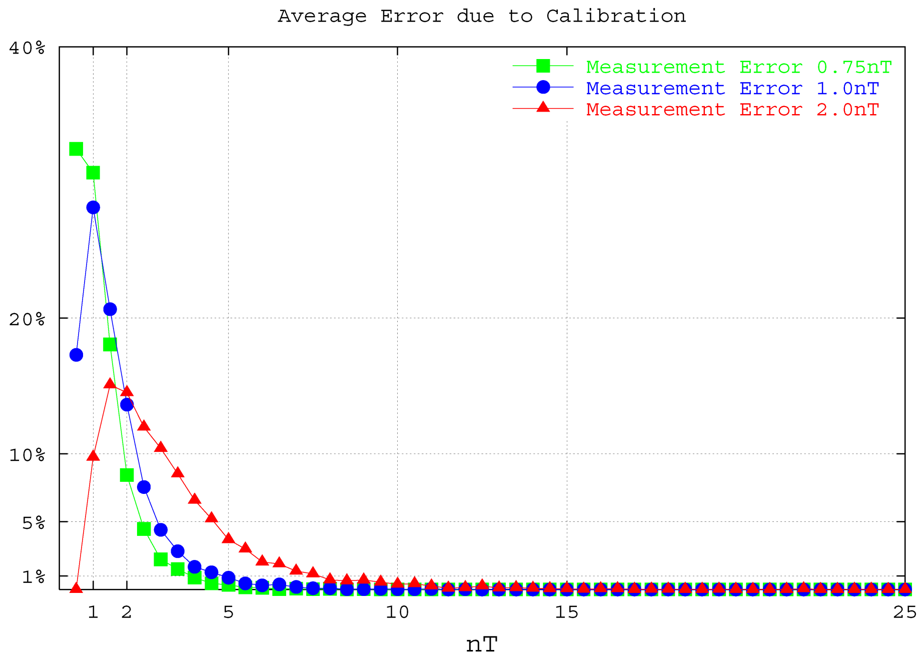

Fig. 5. Normalized histograms of the observed errors for CLF observatory during 1999: the average possible error for $\varepsilon b = 0.75$, 1, 2 nT.

GID
2, 337–363, 2012

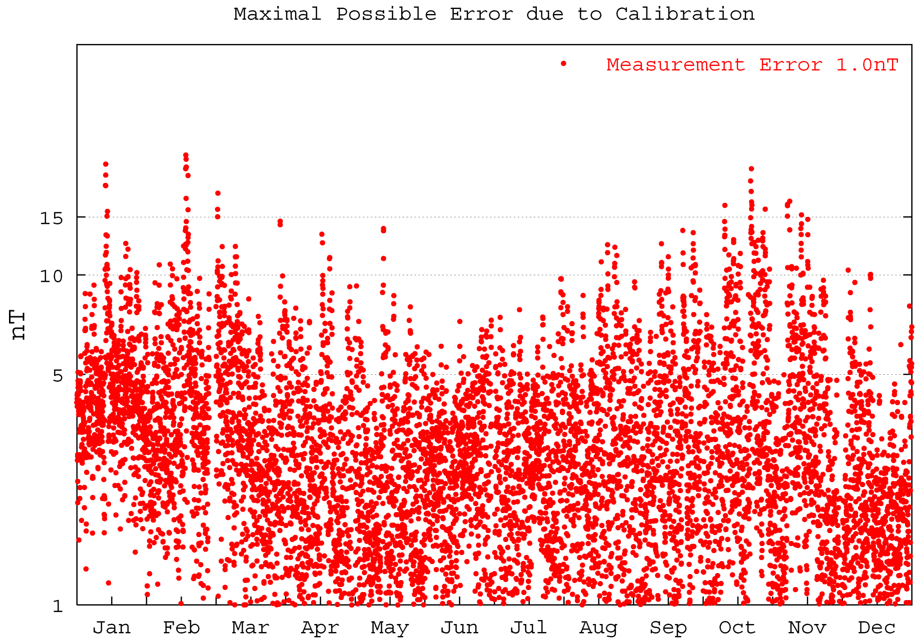

Fig. 6. Sequential observations of the maximal possible calibration error for CLF data, during the year 1999; the value εb is supposed to be 1 nT.

GID
2, 337–363, 2012

Orientation problem for an automatic magnetic observatory

A. Khokhlov et al.

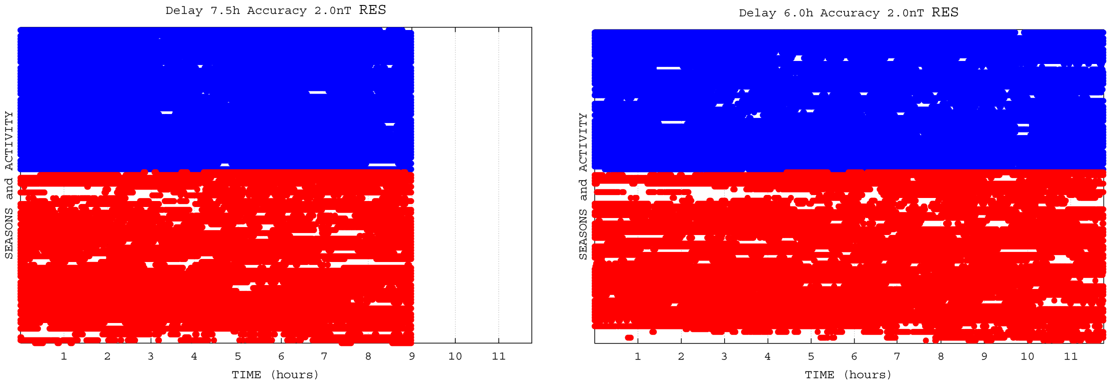

Fig. 7. Time table for RES data, with $t_0 = 7.5\,\mathrm{h}$ (left panel) and $t_0 = 6\,\mathrm{h}$ (right panel) periods for the $\boldsymbol{B}_1(t)$. Note the distinction between subsets $\mathcal{D}_i$ and $\mathcal{Q}_i$: black lines for disturbed days, gray lines for quiet days. Seasonal variation reads in up-to-down (starting with the first five days from January, up to the last five days of December, separately for $\mathcal{D}_i$ and $\mathcal{Q}_i$ families).

GID
2, 337–363, 2012

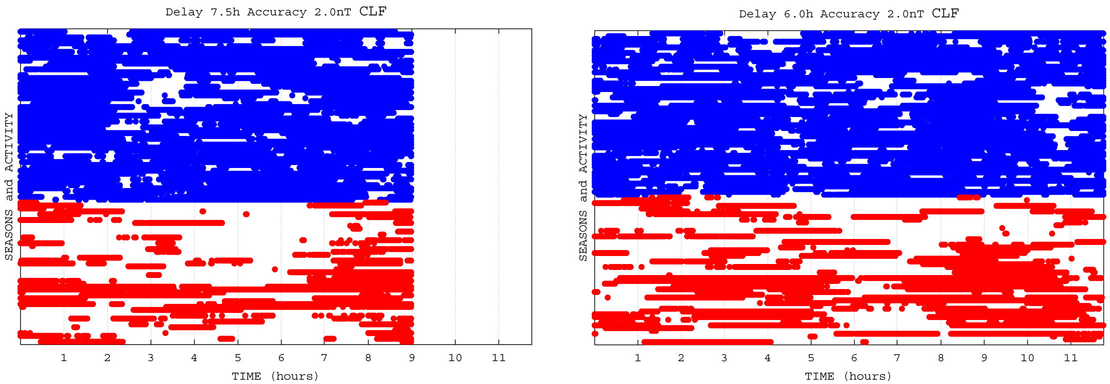

Fig. 8. Time table for CLF data. Same legend as Fig. 7.

GID
2, 337–363, 2012

Orientation problem for an automatic magnetic observatory

A. Khokhlov et al.

Title Page
Abstract Introduction
Conclusions References
Tables Figures
◀◀ ▶▶
◀ ▶
Back Close
Full Screen / Esc
Printer-friendly Version
Interactive Discussion

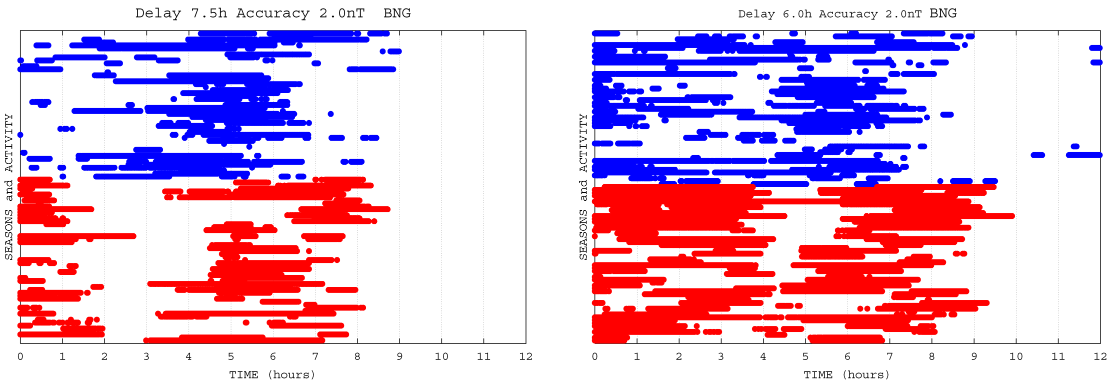

Fig. 9. Time table for BNG data. Same legend as Fig. 7.

GID
2, 337–363, 2012

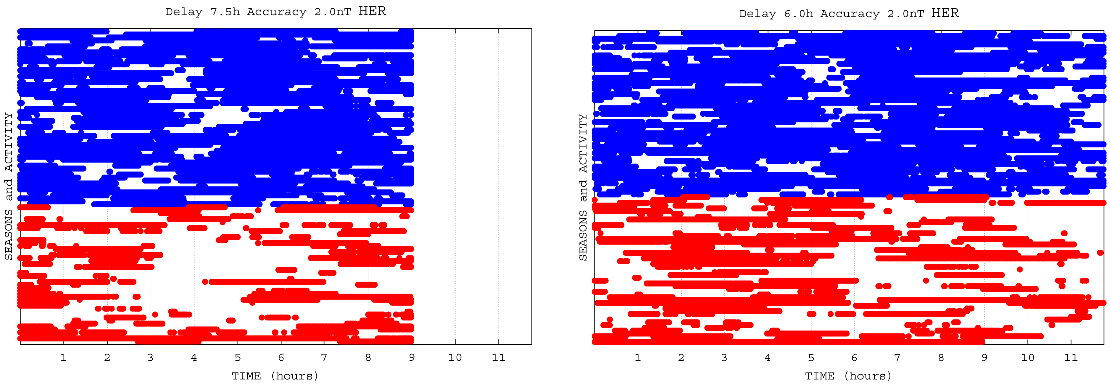

Fig. 10. Time table for HER data. Same legend as Fig. 7.

GID
2, 337–363, 2012

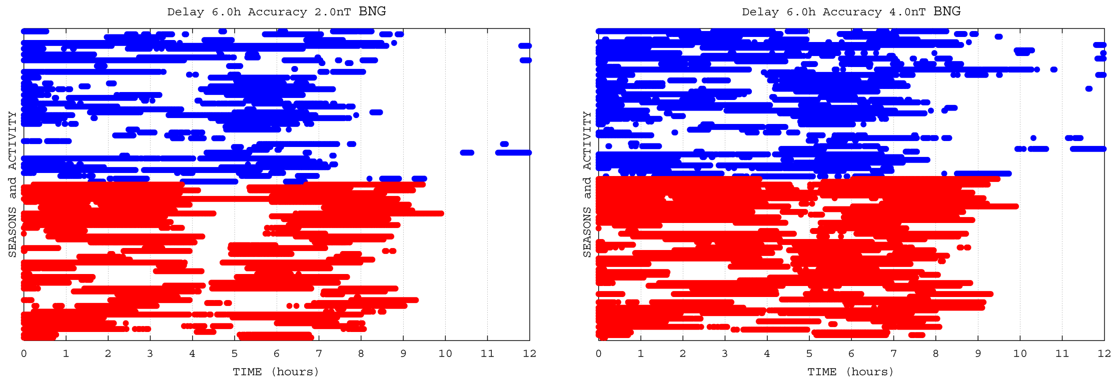

Fig. 11. Time table for BNG data, with $t_0 = 6$ h, "2 nT-good" (left panel) and "4 nT-good" (right panel) periods for the $\boldsymbol{B}_1(t)$. Note the distinction between subsets $\mathcal{D}_i$ and $\mathcal{Q}_i$: black lines for disturbed days, gray lines for quiet days. Seasonal variation reads in up-to-down (starting with the first five days from January, up to the last five days of December, separately for $\mathcal{D}_i$ and $\mathcal{Q}_i$ families).